THE ASTROPHYSICAL JOURNAL, 199:148–165, 1975 July 1

P CYGNI STARS AND MASS LOSS

PUI KUAN AND LEONARD V. KUHI
Department of Astronomy, University of California, Berkeley
Received 1974 November 14

ABSTRACT

The Sobolev approximation is used to compute line profiles formed in rapidly expanding atmospheres. Twelve levels of hydrogen are used in determining the level populations in the envelope under statistical equilibrium. The results are compared to observed hydrogen Balmer series profiles of P Cygni and other stars of similar type. It is found that a decelerating envelope can most adequately account for the observed profiles. Mass loss rates and mechanical momentum fluxes are determined for these stars and correlated with infrared excesses. It is found that low momentum flux favors the presence of dust in the envelope, as indicated by the presence of large infrared excess, whereas high momentum fluxes are found for stars having a free-free infrared emission spectrum.

Subject headings: circumstellar shells — emission-line stars — infrared — line profiles — mass loss

I. INTRODUCTION

It is now a generally accepted interpretation that the presence of P Cygni profiles (emission accompanied by shortward displaced absorption) in the spectra of certain stars is due to the existence of extended expanding envelopes around these stars and consequently that they are ejecting mass into the interstellar medium. There are two related problems associated with this mass loss: (1) How does it affect the star's evolution? (2) What are the properties (gas and dust content) of the interstellar medium in the immediate vicinity of the star? Obviously, to answer these questions, we must have reliable mass loss rates. In this paper, we attempt to determine the mass loss rates from stars with fairly well-defined P Cygni profiles through fitting theoretical hydrogen Balmer line profiles to the observed ones and to correlate them with infrared excesses observed for these stars, which presumably come from the circumstellar envelopes.

Most P Cygni stars are early type supergiants. The discovery of P Cygni profiles in the ultraviolet resonant lines of early supergiants with normal visible spectra by Morton and his co-workers (Morton 1967*a*, *b*; Morton, Jenkins, and Bohlin 1968; Morton, Jenkins, and Brooks 1969) suggests that all early type supergiants may have extended expanding envelopes to some degree. But P Cygni line profiles are by no means restricted to the early type supergiants. In a study by Beals (1951), such diverse objects as the dwarf companion of o Ceti and Z Andromedae, a symbiotic star, are also included in the class of P Cygni stars. Some T Tauri stars, young stars believed to be still contracting to the main sequence, are also known to show P Cygni profiles (Kuhi 1964). The Wolf-Rayet (W-R) stars have extremely broad emission lines, often more than 50 Å wide in the visible part of the spectrum. Sometimes absorption is present, though it is weak and appears only at the extreme shortward end of the emission lines. Loosely speaking, some of them can also be classified as P Cygni profiles. The classical P Cygni profile, on the other hand, has relatively narrow emission compared to the accompanying absorption which is always present and increases in strength with the emission. In a later section, we shall show that the different profiles can be explained quite naturally, at least qualitatively, by line formation in expanding envelopes having different velocity fields: an accelerating one leads to a W-R profile while a decelerating one leads to the classical P Cygni profile.

It would be ideal to start with an ejection mechanism and then to construct a model of an expanding envelope followed by line profile calculations to fit the observed profiles. The Lucy and Solomon theory (Lucy and Solomon 1967, 1970) of mass ejection by the scattering of ultraviolet resonant radiation and a slightly modified theory by Cassinelli and Castor (1973) to include the effect of true absorption seem to be very attractive for early type stars of high luminosity. But in view of the variety of stars we consider in this paper, some of which can hardly be considered luminous, the radiation-driven stellar wind theory very likely fails to apply. Therefore, instead of trying to explain the origin of an extended atmosphere, we simply assume its existence along with some velocity field and compute the line profiles formed in such an envelope. If the assumed velocity field gives a profile that fits the observation, it will give us a clue as to how the extended atmosphere is formed.

Early work on line formation in moving atmospheres include that of Beals (1929, 1930, 1931, 1934), Gerasmovic (1933, 1935), Chandrasekhar (1934) and Wilson (1934). Complete transparency was assumed, and thereby the transfer problem was ignored. Rottenberg (1952) considered line transfer in moving concentric shells. Later it was shown by Sobolev (1958, 1960) that if the macroscopic velocity along the line of sight changes by an amount equal

to the thermal velocity over a distance small compared with the dimension of the envelope, different points on a profile can indeed be considered to have been formed in thin shells or equal-velocity surfaces, within which physical conditions can be assumed uniform. Rublev (1961, 1964) and Lyon (1967) applied Sobolev's theory to the study of W-R spectra. Castor (1970) refined Sobolev's theory and also gave an expression for the mean intensity of line radiation in a velocity surface. Other work, concerned mainly with resonant line scattering in moving atmospheres, include, among others, that of Lucy (1971), Magnan (1970, 1972), Caroff, Noerdlinger, and Scargle (1972), and Noerdlinger and Scargle (1972). While these studies revealed interesting spectral features, they either ignored variation in density and opacity throughout the envelope or assumed arbitrary values for it, and the results were less then adequate for comparison with the vast amounts of observational data. In a series of papers, Hutchings (1968*a*, *b*, 1969) reproduced some observed P Cygni profiles, but he employed an overabundance of parameters which often tended to obscure rather than to elucidate the physical conditions in the atmosphere. Lacking further reliable knowledge of the conditions in an expanding envelope, in this paper we adopt simple assumptions of spherical symmetry, a constant mass ejection rate with the variation in density being determined by the equation of continuity and an assumed velocity law, and statistical equilibrium in atomic level populations governed by radiative and thermal collisional processes. In some cases the resulting profiles reproduce the observed ones quite well, and in others, less adequately. Possible violations of the above assumptions will be discussed.

The correlation between infrared excess and mass loss from early type stars is well known, as evidenced by the work of Johnson (1967), Geisel (1970), Strom *et al.* (1972), and many others. Dyck and Milkey (1972) gave a more detailed description about the evolution of the idea that the infrared excess associated with early type emission-line stars is circumstellar in origin. Although there are still disputes about the actual emission mechanisms in individual stars, Kleinmann and Kuhi (1972) have suggested that there may be a functional relation between mass loss rates and far-infrared excesses. From line profile computations we determine the mass loss rates for a number of stars with P Cygni profiles from Allen's list of early type stars (Allen 1973) of which we have spectrograms and find a well-defined relation between the momentum flux and infrared excess. In general, low momentum flux corresponds to large infrared excess, and the star is often indicated by Allen as having a dusty envelope.

In the next section we briefly review Sobolev's theory on line formation in rapidly moving envelopes and examine the general properties of lines formed in accelerating and in decelerating envelopes. The results will be used to compute detailed profiles to fit the observed Balmer lines of P Cygni. In § III, we determine the mass loss rates of a number of stars and correlate them with their infrared excesses. In § IV, we present arguments for and against the models adopted for the envelopes of the stars we have studied. A summary is provided in the final section.

II. LINE PROFILES

In the absence of scattering, the source function of a line transition between levels i (lower) and j (upper) of frequency ν_{ij} is given by

$$S_{ij} = \frac{2h\nu_{ij}^3}{c^2} \frac{1}{(b_i/b_j)\exp(h\nu_{ij}/kT_e) - 1}, \tag{1}$$

where b_i and b_j are the departure coefficients from LTE of levels i and j, respectively, T_e the local electron temperature, and the other symbols have their usual meanings. For densities of the order of 10^{11} particles per cm^3 in early type stellar envelopes, this is usually considered a good approximation for the subordinate lines but may be unrealistic for resonant lines. For more rigorous calculations, electron as well as resonant line scattering must be included in the evaluation of the source function.

In a rapidly moving atmosphere, when the macroscopic velocity v_z along the line of sight varies by an amount equal to the thermal velocity over a distance interval in which the density and temperature change negligibly, or, according to Rybicki (1970), which is small compared with the photon thermalization length, the Sobolev theory gives the total radiative power per unit frequency per unit solid angle in the z-direction from the envelope as

$$E(\Delta\nu) = \iint S_{ij}\left[1 - \exp\left(-2\kappa_{ij}\rho v_D \Big/ \left|\frac{\partial v_z}{\partial z}\right|\right)\right] dxdy, \tag{2}$$

where $\Delta\nu$ is measured from the rest frequency ν_{ij}. The integral is carried along the velocity surface defined by

$$v_z(x, y, z) = -c\Delta\nu/\nu_{ij}, \tag{3}$$

where κ_{ij} is the mass absorption coefficient, ρ the density, and v_D the thermal velocity in one direction. We have assumed that the line of sight intersects the velocity surface only once. Later we shall give the appropriate expression when the surface is cut twice by the line of sight.

The corresponding photospheric radiation emerging from the envelope on the shortward side of line center is

$$P(\Delta\nu > 0) = R^2 \int_0^{2\pi}\int_0^{\pi/2} I_{ij}^c(\theta') \exp\left(-2\kappa_{ij}\rho v_D \Big/ \left|\frac{\partial v_z}{\partial z}\right|\right) \cos\theta' \sin\theta' d\theta' d\phi, \tag{4}$$

where θ' is the angle between the radius vector and the z-axis, $I_{ij}^c(\theta')$ is the photospheric intensity, and R the photospheric radius. We have referred to the stellar radiation loosely as coming from a photosphere which is in fact ill defined for extended atmospheres. The expression in the exponential is to be evaluated at z, the solution of equation (3) with $x = R \sin\theta' \cos\phi$ and $y = R \sin\theta' \sin\phi$.

The neighboring continuum radiation is simply

$$C = 2\pi R^2 \int_0^{\pi/2} I_{ij}^c(\theta') \cos\theta' \sin\theta' \, d\theta' .$$

The observed normalized profile is

$$\begin{aligned} L(\Delta\nu) &= E(\Delta\nu)/C + 1 , \qquad \Delta\nu \le 0 , \\ &= E(\Delta\nu)/C + P(\Delta\nu)/C , \quad \Delta\nu > 0 . \end{aligned}$$

We have assumed for simplicity that the photospheric radiation is a flat continuum in the neighborhood of the line in question.

For spherically symmetric flows, equation (2) can be transformed to

$$E(\Delta\nu) = 2\pi \int_{r_i}^{r_f} S_{ij}\left[1 - \exp\left(-2\kappa_{ij}\rho v_D \Big/ \left|\frac{\partial v_z}{\partial z}\right|\right)\right] \left|\frac{\partial v_z}{\partial z}\right| \frac{1}{v} r^2 dr , \tag{5}$$

where $\partial v_z/\partial z$ is given by

$$\frac{\partial v_z}{\partial z} = \frac{dv}{dr}\cos^2\theta + \frac{v}{r}\sin^2\theta , \quad v_z = v\cos\theta = -c\Delta\nu/\nu_{ij} . \tag{6a, b}$$

Here v is the radial velocity and θ the angle between a radius vector and the z-axis. The quantities r_i and r_f are the limits of integration and are in general functions of $\Delta\nu$.

When the envelope is optically thin, absorption can be ignored and the line profile becomes

$$L(\Delta\nu) = 2\pi \int_{r_i}^{r_f} (S_{ij}/C) 2\kappa_{ij}\rho v_D v^{-1} r^2 dr + 1$$

for $|\Delta\nu| < \Delta\nu_m = (v_m/c)\nu_{ij}$, where v_m is the maximum velocity of expansion. If the extent of the envelope is large and r_i and r_f can be considered independent of $\Delta\nu$, the line profile is flat-topped and falls abruptly to 1 at both ends. It is quite possible that the flat-topped C III λ5696 line found in early WC stars is formed in such optically thin expanding envelopes (Kuhi 1973).

If the velocity increases linearly with radius, equation (6a) gives a constant $\partial v_z/\partial z$ (independent of $\Delta\nu$). Equation (5) again gives a flat-topped emission profile, but the blueshifted absorption profile depends on the variation of optical depth as a function of $\Delta\nu$, and the center of gravity of the emission is accordingly shifted to the red. In this respect, it differs from the optically thin case.

a) Accelerating Atmospheres

For a spherical accelerating atmosphere, the equal-velocity surface, $v\cos\theta$ = constant, extends from the z-axis through the center of the star to the outside boundary of the envelope. Along the surface, there is a one-to-one relation between r, the radial distance from the center, and θ. Therefore, any line of sight parallel to the z-axis intersects the velocity surface at most only once. Figure 1 shows typical velocity surfaces in an accelerating atmosphere having the velocity structure

$$v = [v_0^2 + v_1^2(1 - R/r)]^{1/2} , \tag{7}$$

where v_0 and v_1 are parameters, and R the photospheric radius.

The occultation effect is relatively unimportant in an accelerating atmosphere if the extent of the emitting envelope is large compared with the size of the central star (which is assumed to be opaque). Let r_f be the radius of the outer boundary of the envelope and v_m the expansion velocity at r_f. The maximum redshifted velocity of emission, v_c, assuming broadening solely due to mass motion, is the solution of

$$\begin{cases} v_f \cos\theta = v_c \\ r_f \sin\theta = R . \end{cases}$$

Eliminating θ, we get

$$v_c/v_m = [1 - (R/r_f)^2]^{1/2} . \tag{8}$$

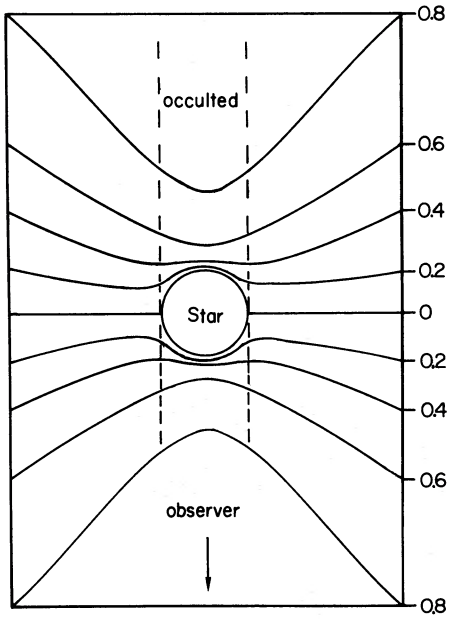

FIG. 1.—Equal velocity surfaces of an accelerating atmosphere. The numbers beside the curves indicate the ratio v_z/v_m where v_m is the maximum expansion velocity.

For $r_f \gg R$, $v_c/v_m \sim 1$. The blueshifted absorption edge gives v_m while the redshifted emission edge gives v_c. If the envelope is strictly accelerating, then if v_m and v_c are known, equation (8) gives the size of the envelope.

When the velocity surfaces have large optical depths, the emission integral (5) can be approximated by

$$E(\Delta\nu) = 2\pi \int_{r_i}^{r_f} S_{ij}\left(\left|\frac{\partial v_z}{\partial z}\right| \Big/ v\right) r^2 dr = 2\pi \int_{r_i}^{r_f} S_{ij}\left|1 - (v_z/v)^2\left(1 - \frac{r}{v}\frac{dv}{dr}\right)\right| r dr \,. \tag{9}$$

The upper limit is a constant, but the lower limit depends on $\Delta\nu$, or v_z. Let Δr denote the maximum variation in r_i as $\Delta\nu$ changes. If $(r_f - r_i) \gg |\Delta r|$, where $\bar{r}_i$ is some average r_i, for all $\Delta\nu$, and the source function does not vary rapidly in the interval $(\bar{r}_i, \bar{r}_i \pm \Delta r)$, then r_i can be replaced by $\bar{r}_i$. We further assume that most of the acceleration takes place close to the photosphere and approaches the terminal velocity v_m at $r \ll r_f$, so we can approximate (9) by

$$E(\Delta\nu) = 2\pi \int_{\bar{r}_i}^{r_f} S_{ij} r dr[1 - (v_z/v_m)^2] = \pi \bar{S}_{ij} r_f^2 [1 - (\Delta\nu/\Delta\nu_m)^2] \,, \qquad \Delta\nu_m = \frac{v_m}{c}\nu_{ij} \,,$$

where $\bar{S}_{ij}$ is approximately a weighted average of S_{ij} with weight r over the interval $(\bar{r}_i, r_f)$. The emission profile is seen to be an inverted parabola. Since the envelope is assumed to be optically thick, the radiation from the photosphere can be regarded as being totally removed by the intervening envelope on the blue side of the line center up to the maximum frequency shift. For simplicity we assumed that I_{ij}^c is a constant across the stellar disk. The normalized profile is then

$$L(\Delta\nu) = \frac{\bar{S}_{ij} r_f^2}{I_{ij}^c R^2}[1 - (\Delta\nu/\Delta\nu_m)^2] + \begin{cases} 1 \,, & \Delta\nu \le 0 \,, \\ 0 \,, & \Delta\nu > 0 \,. \end{cases} \tag{10}$$

As the emission strength increases, either due to an increase in the extent of the envelope or the average source function, the portion of the profile below the continuum is progressively pushed toward the shortward edge. More precisely, $L(\Delta\nu)$ falls below unity if

$$1 \ge \Delta\nu/\Delta\nu_m > \left[1 - \left(\frac{I_{ij}^c R^2}{\bar{S}_{ij} r_f^2}\right)^2\right]^{1/2} . \tag{11}$$

In the spectra of W-R stars, the emission is often many times stronger than the continuum, while the absorption edge is barely visible or completely absent. Line formation in a rapidly accelerating atmosphere of large extent naturally explains the origin of such a line profile. On the other hand, if the physical assumptions leading up to (10) and (11) are realized, a P Cygni profile of strong longward emission with broad and deep shortward absorption cannot be formed in an accelerating atmosphere regardless of the detailed velocity law.

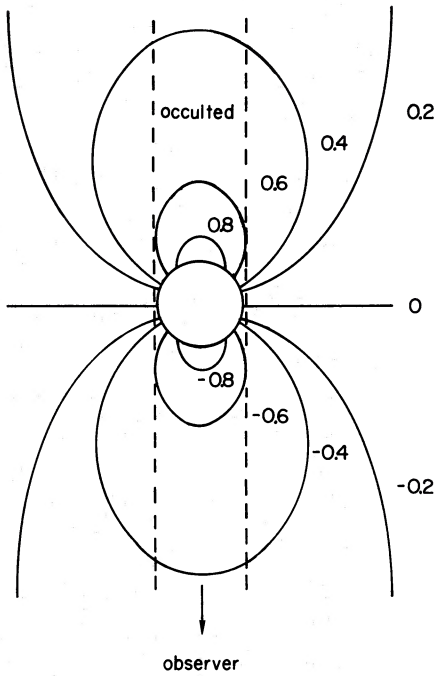

FIG. 2.—Equal velocity surfaces of a decelerating atmosphere. The numbers beside the curves indicate the ratio v_z/v_0. The velocity law is $v_0(R/r)^{1/2}$.

b) *Decelerating Atmospheres*

We take a simple decelerating velocity law,

$$v(r) = v_0(R/r)^l , \tag{12}$$

where $l > 0$ and is used as a deceleration parameter, v_0 is a constant, and R is the photospheric radius. Some equal-velocity surfaces for $l = \frac{1}{2}$ are shown in Figure 2.

The line of sight represented by $r \sin\theta = t$ intersects the velocity surface $v_z = v \cos\theta$ at r, which is the solution of the following equation obtained by eliminating θ and using (12):

$$(t/R)^2(R/r)^{2(l+1)} - (R/r)^{2l} + (v_z/v_0)^2 = 0 . \tag{13}$$

All velocity surfaces originate at the photosphere. Inside the cone, $\theta = \theta_c = \sin^{-1}[l/(l+1)]^{1/2}$, as r increases, the surfaces move toward the z-axis while outside the cone they move away from it. A line of sight may cut a velocity surface once or twice at $r > R$, or not at all. If we count only the number of solutions to equation (13) for $r > R$, it can be shown that for

$$|v_z/v_0| > [1/(l+1)]^{1/2} \quad \text{and} \quad 0 \le t < [1 - (v_z/v_0)^2]^{1/2}R ,$$

one solution exists; for other values of t, there is no solution.

For $|v_z/v_0| < [1/(l+1)]^{1/2}$ and $0 \le t < [1 - (v_z/v_0)^2]^{1/2}R$, again one solution exists; for the same range of v_z/v_0 and

$$R_d[l/(l+1)]^{1/2} > t > R[1 - (v_z/v_0)^2]^{1/2} ,$$

however, there are now two distinct solutions; $R_d > R$ is a double root of (13) for values of $|v_z/v_0| < [1/(l+1)]^{1/2}$ and for $t = r[l/(l+1)]^{1/2}$; for any other value of t, no solution exists.

Since all velocity surfaces curve back toward the z-axis, the occultation effect becomes important. The line of sight $t = R$ is tangent to the velocity surface $v_z = v_c$ for which equation (13) has a double root. For any $v_z > v_c$ the surface lies totally behind the star and is hence unobservable. The velocity v_c is given by

$$v_c/v_0 = [l/(l+1)]^{l/2}[1/(l+1)]^{1/2} . \tag{14}$$

Table 1 shows v_c/v_0 as a function of l.

TABLE 1

CUTOFF VELOCITY AS A FUNCTION OF THE DECELERATION PARAMETER l

l	1/6	1/5	1/4	1/3	1/2	1	3/2
v_c/v_0	0.787	0.763	0.731	0.687	0.620	0.500	0.431

If a spectral line were formed in a decelerating atmosphere which can be approximated by a power law, v_0 can be obtained from the displacement of the shortward edge and v_c from that of the longward edge, assuming that macroscopic motion is the dominant broadening mechanism. From equation (14), the exponent can be calculated.

The integration of the emission and absorption profiles has to be modified since a line of sight may intersect an equal-velocity surface up to two times. When R_d lies on a surface, the integration is broken into two parts, one from r_i to R_d, the other from R_d to r_f. On the shortward side, r_i is equal to R for all $\Delta\nu$ up to $\Delta\nu_m = (v_0/c)\nu_{ij}$ and r_f is the smaller value between the solution of (13) with $t = 0$ and the maximum radius R_m of the envelope. On the longward side, both r_i and r_f are solutions of (13) with $t = R$ for $|\Delta\nu| < (v_c/c)\nu_{ij}$. To simplify our notation, we denote $2\kappa_{ij}\rho v_D/|\partial v_z/\partial z|$ by τ. The emission integral is

$$E(\Delta\nu > 0) = 2\pi\left[\int_R^{R_d} S_{ij}(1 - e^{-\tau(r)})e^{-\tau'(r')}\left(\left|\frac{\partial v_z}{\partial z}\right|/v\right)r^2dr + \int_{R_d}^{r_f} S_{ij}(1 - e^{-\tau(r)})\left(\left|\frac{\partial v_z}{\partial z}\right|/v\right)r^2dr\right],$$

$$E(\Delta\nu < 0) = 2\pi\left[\int_R^{R_d} S_{ij}(1 - e^{-\tau(r)})\left(\left|\frac{\partial v_z}{\partial z}\right|/v\right)r^2dr + \int_{r_d}^{r_f} S_{ij}(1 - e^{-\tau(r)})e^{-\tau'(r')}\left(\left|\frac{\partial v_z}{\partial z}\right|/v\right)r^2dr\right]. \quad (15)$$

The optical depth τ' is to be evaluated at r' which is the other solution of (13) (the first being r) with

$$t = r[1 - (v_z/v_0)^2(r/R)^2]^{1/2}.$$

The intensity at the center of the line is obtained by integrating along the straight line through the center of the star and perpendicular to the line of sight from R toR_m using (6).

Transforming cos θ' to μ, the absorption profile takes the form

$$P(\Delta\nu > 0) = 2\pi R^2 \int_0^1 I_{ij}^c(\mu) \exp[-(\tau_1 + \tau_2)]\mu d\mu, \quad (16)$$

where τ_1 and τ_2 are to be evaluated at r_1 and r_2, respectively, which are the solutions of (13) with $t = R(1 - \mu^2)^{1/2}$, provided that r_1 and r_2 exist and lie between R and R_m; otherwise the τ's are taken to be zero.

We have found earlier that for $v_z > v_c$, all the equal-velocity surfaces are occulted by the stellar disk. By symmetry, all the velocity surfaces with $v_z < -v_c$ lie directly between the star and the observer. Consequently the extent of these surfaces does not exceed $2R$ in the direction perpendicular to the line of sight. In a crude analysis, these surfaces can be considered as straight segments directly in front of the star. The line profile for $\Delta\nu > (v_c/c)\nu_{ij} = \Delta\nu_c$ is approximately

$$E(\Delta\nu) + P(\Delta\nu) = 2\pi\int_0^{R'} S_{ij}(1 - e^{-\tau})xdx + 2\pi R^2\int_0^1 I_{ij}^c e^{-\tau}\mu d\mu = \pi R'^2 S_{ij}[1 - \exp(-\bar{\tau})] + \pi R^2 \bar{I}_{ij}^c e^{-\tau},$$

$$0 < R' < R,$$

where the barred values represent averages. The normalized profile is

$$L(\Delta\nu > \Delta\nu_c) = \frac{R'^2\bar{S}_{ij}}{R^2\bar{I}_{ij}^c}[1 - \exp(-\bar{\tau})] + \exp(-\bar{\tau}). \quad (17)$$

If $\bar{S}_{ij}$ does not exceed $\bar{I}_{ij}^c$, it is obvious that $L(\Delta\nu > \Delta\nu_c)$ is always less than unity irrespective of the optical depths. For large values of τ, the residual intensity is roughly the ratio of the source function in the envelope to the average intensity in the neighboring continuum.

The above results apply equally well to non–power-law decelerating atmospheres, for they require only that the velocity surfaces start from the photosphere and end up on the central z-axis. The precise cutoff velocity, v_c, depends on the particular velocity law. A typical profile in such an atmosphere will be as follows, assuming $\bar{S}_{ij} < \bar{I}_{ij}^c$: longward of $\Delta\lambda_c$ [i.e., for $\Delta\lambda > (v_c/c)\lambda_{ij} = \Delta\lambda_c$], emission from the envelope is occulted by the stellar disk and we see only the stellar continuum; shortward of $-\Delta\lambda_c$, the line intensity falls below the continuum up to the maximum wavelength or shift, $-(v_c/c)\lambda_{ij}$. These properties of the line profile, it must be noted, do not depend on the central intensity of the line. Thus we can have emission many times above the continuum while the residual flux

in the accompanying absorption can practically go to zero. These are in fact the salient features of typical P Cygni profiles.

c) *Computation of Line Profiles*

The electron temperature in a steadily expanding atmosphere is determined by the balance of various heating and cooling mechanisms. In general, besides heating by stellar ultraviolet radiation we can also expect mechanical heat input since some sort of instability must exist to initiate an outflow. The envelope cools through expansion and radiation loss in the optically thin parts of the spectrum. Since the nature and amount of mechanical heat input are quite uncertain and subject to diverse speculations, we adopt the following scheme for the electron temperature structure for the envelope (which may or may not have physical significance): the expanding gas cools adiabatically from the photospheric temperature to a minimum determined by stellar Lyman continuum heating, with the envelope being assumed optically thick to its own Lyman continuum radiation. In the subsequent statistical equilibrium calculations it is found that the level populations are determined mainly by photoionization from the ground state followed by recombination to higher levels. The local electron temperature has little effect on the opacity and line source functions.

Ignoring recombination to the ground state (since the envelope is assumed to be optically thick to its own Lyman continuum radiation), the net radiative rate, R_i, into level i is given by

$$R_i = \sum_{j=i+1}^{q} (N_j A_{ji} + N_j 4\pi B_{ji}\langle J_{ij}\rangle - N_i 4\pi B_{ij}\langle J_{ij}\rangle)/(h\nu_{ij}) - \sum_{1\le k<i} (N_i A_{ik} + N_i 4\pi B_{ik}\langle J_{ik}\rangle$$
$$- N_k 4\pi B_{ki}\langle J_{ik}\rangle)/(h\nu_{ik}) + \begin{cases} N_e N_p \alpha_i & (i \neq 1) \\ 0 & (i = 1) \end{cases}$$
$$- N_i 4\pi \int_{\nu_i}^{\infty} a_i(\nu)(J_\nu^c/h\nu)\left(1 - \frac{1}{b_i}\exp\left[-h\nu/(kT_e)\right]\right) d\nu\,, \tag{18}$$

where q is the maximum number of levels considered; N_i the number density in level i; A_{ij}, B_{ij} the Einstein A and B coefficients; N_e, N_p the electron and proton number densities; α_i the recombination coefficient; a_i the ionization cross section from level i; ν_{ij} the transition frequency between levels i and j; ν_i the frequency at the ionization edge of level i; J_ν^c approximately the stellar continuum radiation which is assumed to have a blackbody spectrum diluted by geometry effects, and $\langle J_{ij}\rangle$ according to Castor (1970) is given by

$$\langle J_{ij}\rangle = (1 - \beta_{ij})S_{ij} + \beta_{ij}^c I_{ij}^c, \qquad \beta_{ij} = [1 - \exp(-\bar{\tau}_{ij})]/\bar{\tau}_{ij}\,, \quad \beta_{ij}^c = \tfrac{1}{2}\{1 - [1 - (R/r)^2]^{1/2}\}\beta_{ij}\,,$$
$$\bar{\tau}_{ij} \approx \frac{\pi e^2}{mc}(f\lambda_{ij})N_i^*\{b_i - b_j \exp\left[-h\nu_{ij}/(kT_e)\right]\}\frac{r}{v}\,, \tag{18a}$$

where N_i^* is the LTE number density if the electron temperature is T_e, and b_i the departure coefficient of level i from the LTE value, i.e., $N_i = b_i N_i^*$.

The net collision rate is

$$\mathscr{C}_i = \sum_{j\neq i} (N_j N_e C_{ji} - N_i N_e C_{ij}) + N_p N_e C_{\kappa i} - N_i N_e C_{\kappa i}\,. \tag{19}$$

The C_{ij}'s are the collisional cross sections multiplied by the relative velocity of collision averaged over a Maxwellian velocity distribution; κ denotes the continuum. The excitation rates are calculated from formulae and values given by Allen (1963); for C_{ik}, we use a formula given by Mihalas (1970) and the cross sections given by Percival (1966). N_p is the proton number density.

Under statistical equilibrium,

$$R_i + \mathscr{C}_i = 0, \qquad i = 1, 2, \ldots, q\,. \tag{20}$$

The above equation can be transformed to a system of equations with the departure coefficients, the b_i's, as unknowns, i.e.,

$$\sum_j a_{ij}(b_1, \ldots, b_q) b_j = c_i, \qquad i = 1, \ldots, q\,, \tag{21}$$

where the coefficients a_{ij} depend on the b_i's through the escape probabilities β_{ij}, and the c_i's are constants. The system (21) can be solved by successive approximation as follows: Let

$$b_i = b_i^0 + b_i^1 + \cdots, \qquad a_{ij}^0 = a_{ij}(b_1^0, b_2^0, \ldots, b_q^0)\,, \quad \frac{\partial a_{ij}^0}{\partial b_k} = \frac{\partial a_i}{\partial b_k}$$

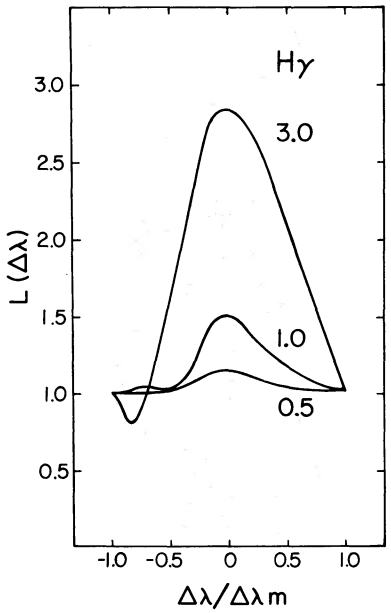

FIG. 3.—Hγ profiles in an accelerating atmosphere for different mass loss rates which are shown beside the curves in units of $10^{-6}\ M_\odot\ \mathrm{yr}^{-1}$.

evaluated at $(b_1^0, \ldots, b_p^0)$. First-order expansion of (21) gives

$$\sum_k \left(\sum_i \frac{\partial a_{ij}}{\partial b_k} b_j^0 + a_{ik}^0 \right) b_k^1 = c_i - \sum_j a_{ij}^0 b_j^0 . \tag{22}$$

The zeroth-order values of the b_i's are guessed at initially, and the true values are obtained by successive approximation using (22). The above method converges rapidly, and in most cases five iterations give an accuracy better than 1 percent.

In the numerical computations of line profiles, a stellar radius and temperature are chosen and a constant mass loss rate is assumed. The density and temperature structures in the envelope are determined by the equation of continuity and the scheme outlined at the beginning of this section. The departure coefficients are evaluated at a

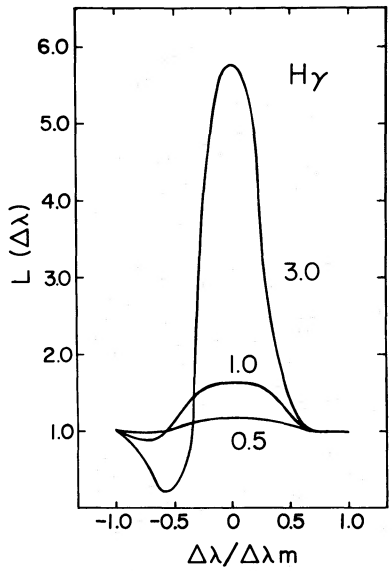

FIG. 4.—Hγ profiles in a decelerating atmosphere for different mass loss rates which are shown beside the curves in units of $10^{-6}\ M_\odot\ \mathrm{yr}^{-1}$.

large number of points (typically 50) in the envelope, and intermediate values are interpolated linearly between adjacent points. The emission integral is evaluated by Simpson's rule, and the residual photospheric intensity is evaluated either by Simpson's rule or a Gaussian quadrature when the integral in μ extends from 0 to 1. The usual LTE limb-darkening law in the Eddington approximation is used for the photospheric intensity. An accuracy of 5 percent in the final profile is aimed at in the numerical computations. When 12 levels of H are considered, a profile on the average takes $\sim$40 seconds on the CDC 6400.

d) Result and Application to P Cygni

Line profiles are computed for accelerating and decelerating models. Figure 3 shows the Hγ profiles for different mass loss rates using the accelerating law (7) with $v_0 = 100$ km s^{-1} and $v_1 = 300$ km s^{-1}. The photospheric temperature and absolute bolometric magnitude are taken to be 30,000 K and -7.4, respectively, corresponding to a photospheric radius of 10 $R_\odot$. Figure 4 shows Hγ profiles in a decelerating atmosphere having the velocity law (12) with $l = \frac{1}{2}$ and $v_0 = 3000$ km s^{-1}. The photospheric temperature and radius, and the mass loss rates, are the same as those used in computing Figure 3. In all cases a composition of 64 percent H and 36 percent He by mass is assumed. Both H and He are assumed to be totally ionized in calculating the electron densities. The endpoint of integration is taken to be $10R$, beyond which contributions become negligible.

The first point to note from the figures is that the emission intensities are very sensitive to the mass loss rate. This results from the fact that the opacity is roughly proportional to the square of the density which in turn is proportional to the mass loss rate. Thus the fitting of profiles to observations can be a very accurate means of determining mass loss from P Cygni type stars.

In the profiles of the accelerating model, emission extends to the maximum velocity of expansion. Occultation plays an insignificant role since the velocity surfaces are large and only a small fraction of them lies behind the star. Absorption below the continuum may or may not be present, but this does not mean that the envelope is necessarily thin. Careful inspection of the Hγ profile with a mass loss rate of $3 \times 10^{-6}\ M_\odot\ \mathrm{yr}^{-1}$ shows that at a point on the shortward side, the intensity can be as much as 0.7 below that of a symmetrical point on the longward side. The emission from the envelope simply fills up the absorption of photospheric radiation. For strong lines, the wavelength shift at which the intensity falls below the continuum has been estimated earlier to be $\Delta\lambda \sim (1 - 1/E_0^2)^{1/2}\Delta\lambda_m$, where E_0 is the intensity above the continuum at the center of the line and $\Delta\lambda_m$ the maximum wavelength shift. This is borne out in the numerical computation. We also notice that the profiles are round-topped. We have found that if the envelope is optically thin, the profiles should be flat-topped when the emission integral is independent of the initial point of integration. The reason that this is not so in our calculations is that the envelope accelerates rapidly at the base, causing the density to fall off sharply. For a thin envelope, the main contribution to the emission integral comes from the region near the photosphere and therefore depends strongly on the initial point of integration. This results in the round-topped profiles we have produced.

In the profiles of the decelerating model, the conspicuous feature is the longward cutoff in emission. The velocity shift at which the cutoff occurs depends solely on the velocity law used, which determines the geometry of the velocity surfaces. Since we have used a decreasing temperature structure for the envelope and no population inversion is found for the levels considered, absorption below the continuum is always present for velocity shifts beyond $-v_c$ defined by equation (14). The absorption and emission strengths both increase with optical depth. For the strongest line shown in Figure 4, the residual intensity is only about 20 percent, while the emission intensity goes more than 5 times that of the continuum. Another characteristic of the profiles is that for large optical depths the emission peak is rounded whereas for small optical depths it becomes flat. Since the integration for all velocity shifts starts from R, it is understandable that the profile should become flat-topped for optically thin envelopes according to the analysis at the beginning of this section. Comparing accelerating and decelerating model profiles, we notice that for the same mass loss rate, the central intensity is consistently higher for the decelerating model profile. This is because the density decreases less rapidly in a decelerating envelope and the size of the envelope which contributes significantly to the emission is consequently larger.

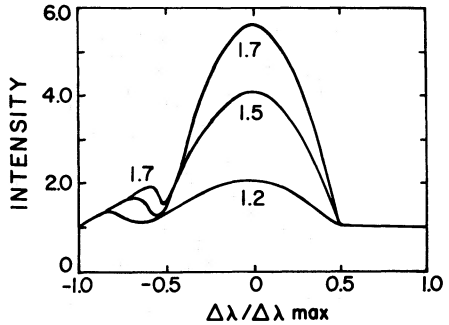

FIG. 5.—Artificial line profiles. For explanation, see text.

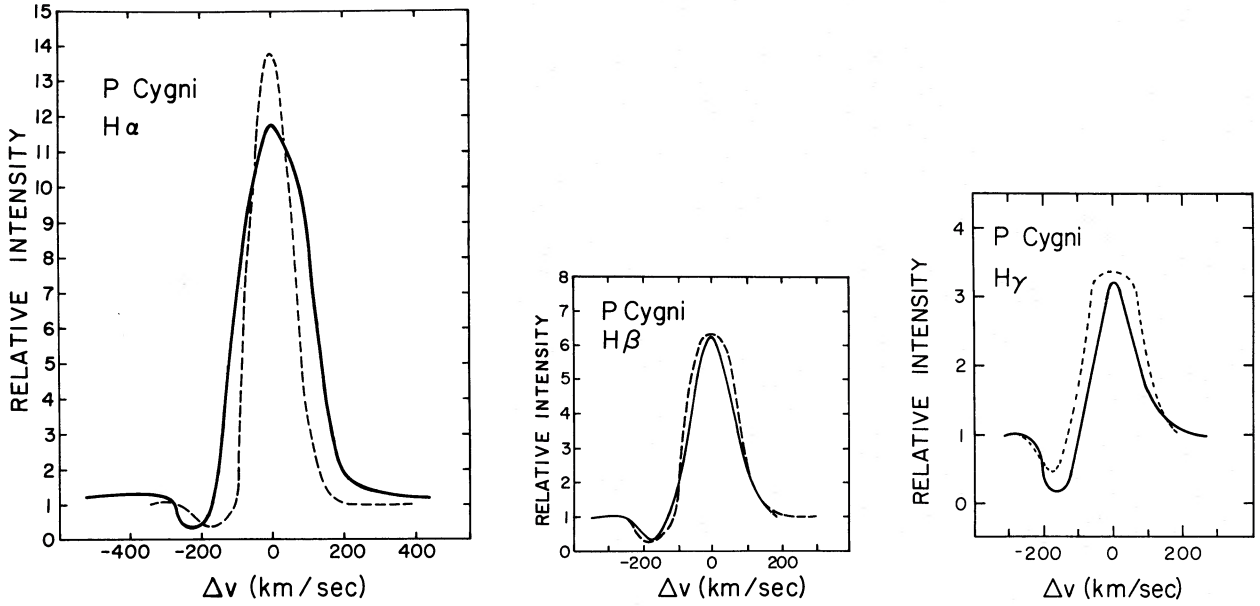

FIGS. 6*a*, *b*, *c*.—Observed (*solid*) and computed (*dashed*) Hα, Hβ, Hγ profiles of P Cygni

Figure 5 shows some profiles formed in extremely artificial expanding atmospheres. The velocity law used is $v = v_0(R/r)$, and the opacities are assumed to be infinite. The star's temperature is 30,000 K while that of the envelope is a constant 50,000 K. The extent of the envelope goes from R to $1.2R$, $1.5R$, and $1.7R$, and is shown alongside the profiles. The interesting feature is a secondary maximum on the shortward side of each profile. This comes about because for an infinite opacity and a constant-temperature model the emission is strictly proportional to the projected area of a velocity surface. For the models adopted above, the surfaces have two relative maxima in projected area, which show up as two emission peaks in the profile (a third one on the longward side being occulted). Although the model may explain the splitting of emission lines (Rublev 1964), considerable discretion must be exercised before applying it to observations because of its highly arbitrary nature.

Blue and red spectrograms of P Cygni at 16 Å mm^{-1} were obtained with the 20-inch (51 cm) coudé camera at Lick Observatory in 1971. The edges of Hβ and the higher members of the Balmer series show longward and shortward displacements of $\sim$200 and 280 km s^{-1}, respectively, from the central emission peaks. The displacements of the peaks themselves from a standard frame of reference (with respect to the Sun) have a dispersion of about 10 km s^{-2}. For the lower members of the series the emission strengths are very strong and the residual intensities in the absorption components are not far from zero. This suggests that the lines may be formed in a decelerating atmosphere whose velocity structure can be approximated by $v \propto 1/r^{1/2}$ (see Table 1). The maximum expansion velocity at the base of the envelope is 280 km s^{-1} as indicated by the velocity shift of the shortward edge from the line center. Occultation effects give a longward cutoff at $\sim$180 km s^{-1}. Before we compare theoretical profiles with observed ones, it is appropriate to reiterate our assumptions. The envelope is assumed to be steadily expanding and to possess spherical symmetry. The base of the envelope is taken to be a sphere of radius R emitting blackbody radiation of temperature T_c, the color temperature of the star. The envelope cools off as it expands to a minimum electron temperature $T_{\min}$ determined by stellar Lyman continuum heating and cooling through recombination to levels higher than the ground state. The density in the envelope is determined by an assumed constant mass loss rate and the equation of continuity. The level populations are obtained by solving the statistical equilibrium equations using the escape probability method to determine the average intensities of line radiation. The intrinsic line profile of a transition is assumed to be a rectangular one with the width corresponding to the average thermal broadening velocity. The integration is carried to large radii beyond which contributions become negligible.

According to Beals (1951) and Kopylov (1958), the stellar temperature and absolute magnitude of P Cygni are 30,500 K and -8.4, respectively, corresponding to a stellar radius of 15.2 $R_\odot$. The minimum temperature in the envelope based on our assumptions is about 19,000 K. From the displacements of the edges of Hβ, Hγ, and Hδ profiles, we deduce the velocity law $v = 280(R/r)^{1/2}$ km s^{-1}. The mass loss rate is used as a free parameter to fit the observed emission intensity of Hβ. Using the same parameters, profiles of the other Balmer lines are also computed. The resulting profiles of Hα, Hβ, and Hγ are shown in Figure 6 along with the observed ones, using a mass loss rate of $3.4 \times 10^{-6}\ M_\odot\ \mathrm{yr}^{-1}$. In all cases, the emission peaks are considered to be the line centers. Figure 7 shows the optical depths $\bar{\tau}_{ij}$ and the source functions S_{ij} divided by $2h\nu_{ij}^3/c^2$ as functions of r. Twelve levels of H have been considered.

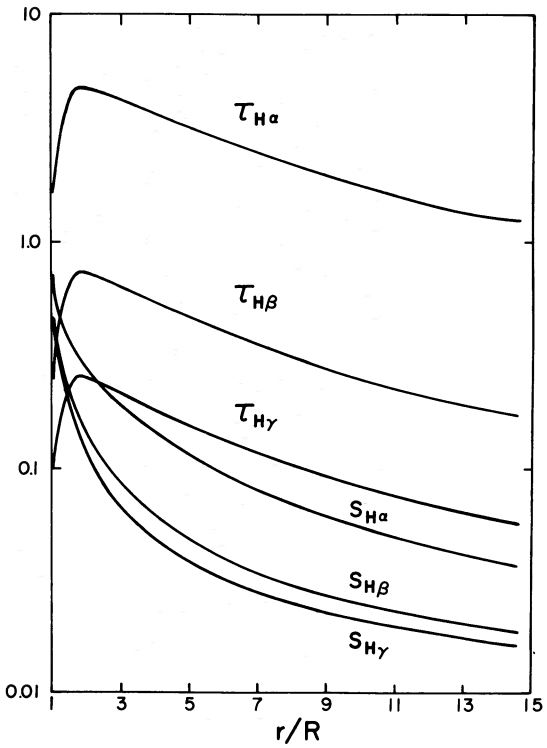

FIG. 7.—Optical depths and source functions of Hα, Hβ, and Hγ in the envelope of P Cygni

The computed profiles do not fit the observed ones exactly. For the higher Balmer lines where the envelope becomes optically thin, the computed profiles are flat-topped but the observed ones are peaked and also have deep absorption cores. For Hα the observed profile is noticeably wider by about 50 km s^{-1} and has extensive emission wings. It is possible that the latter feature can be explained by noncoherent electron scattering in the atmosphere (Castor, Smith, and van Blerkom 1970). For the weaker lines, we expect the assumption of a simple decelerating atmosphere to break down since the envelope has to be somehow accelerated to the maximum velocity which allows the gas to escape from the star. When the outer envelope becomes transparent, the lines will be formed predominantly in the accelerating part of the atmosphere. Since the longward emission edge is much closer to the central emission peak than the shortward absorption edge for the weaker lines which we assume to have contributions from the accelerating part of the envelope, the occultation effect is significant and the acceleration must be rapid according to equation (8). Consequently the emitting volume is small and will give a weak but sharp peak. The amount of absorption depends largely on the opacity, and the filling-in by emission is relatively unimportant. From these qualitative pictures it is hoped that once we know how the envelope is being accelerated, profile fitting will be considerably improved.

Despite the shortcomings of the theoretical profiles, one notes that the computed central intensities are remarkably close to the observed one. We have shown only three profiles, but for the higher Balmer lines the theoretical central intensities all lie within 20 percent of the observed values. (Observed Hα, Hβ, Hγ, Hδ central relative intensity: 11.8, 6.3, 3.2, 2.2; computed, 13.8, 6.3, 3.3, 2.2.) For the strong lines (Hα, Hβ), when one cannot observe through the decelerating outer envelope, the minimum residual intensities agree very well with the observed ones. In passing, we note that when LTE is assumed (with the same temperature structure), we can duplicate neither the Balmer decrement nor the deep absorption cores of the stronger lines (none gets more than 40 percent below the continuum). Also the optical depths found here for the lines have properties (i.e., a single maximum) similar to the function assumed by Castor (1970) in an attempt to produce approximately symmetric profiles.

III. MASS LOSS AND INFRARED EXCESS

The relative success of our model for P Cygni in reproducing the observed line profiles has prompted us to determine the mass loss rates for a number of stars having similar profiles. The Balmer lines of BD+61°154 and CoD−27°11944, in particular, closely resemble those of P Cygni in having well-defined emission and absorption components and little sign of the presence of the underlying photospheric lines. In others, the Stark-broadened extensive wings of the photospheric lines are clearly present. Figure 8 shows a smoothed observed Hγ profile of

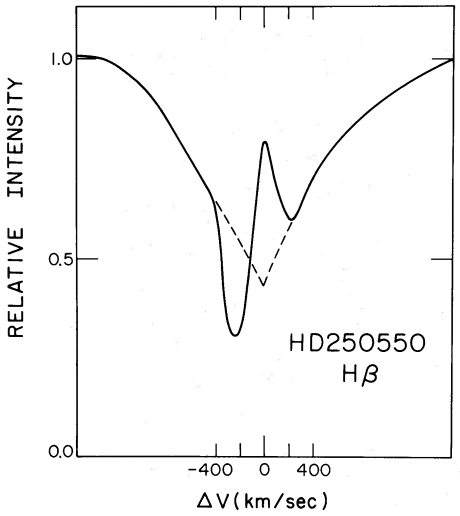

FIG. 8.—Observed Hγ profile of HD 250550. The dashed curve shows what the line profile would be in the absence of an expanding envelope.

HD 250550 obtained from a spectrogram of 16 Å mm^{-1} dispersion. For such cases, it is not obvious how the part of the profile formed in the expanding envelope should be separated from that coming from the photosphere. Lacking a refined theory, the following crude procedure was used. The Stark-broadened wings are extrapolated toward the central core which often coincides with the emission peak as shown by the dashed curve in Figure 8. The points at which the dashed curve meets the observed profile defines the velocity shifts of the edges of the line formed in the expanding envelope. The central emission intensity is measured from the peak to the Stark-broadened core. When this intensity is divided by the intensity of the neighboring continuum and has 1 added to it, it gives the relative intensity of emission from the envelope. The velocity shifts, $+\Delta v_r$, $-\Delta v_b$, their ratio K, and the relative central intensities of Hβ, Hγ, Hδ for the stars observed are shown in Table 2.

Some of the profiles either are too weak to be measured or have velocity shifts that cannot be determined reliably due to the presence of secondary emission features. These values are omitted from the table. For Z CMa, emission shows up on the longward wing of the Stark-broadened profile. It may be that the whole photosphere is accelerating upward, producing a shortward shifted absorption line. It can also be interpreted, using the Sobolev theory, to mean that the absorption line is unshifted but the emission from the envelope is shifted due to expansion as well as rotation. For MWC 342, it seems that the profile is one of symmetric emission mutilated on the shortward side by absorption by a slower-moving shell. These atypical profiles are shown in Figures 9 and 10, respectively. All the other profiles are either like those of P Cygni or like the one shown in Figure 8.

Whenever measurable, it is seen from Table 2 that K, the ratio of the velocity shifts of the longward and shortward edges from the central emission peak of a spectral line, is remarkably close to 0.62, a value that corresponds to a decelerating envelope having velocity $v \propto r^{-1/2}$. We have selected these stars not because of the fact that their K values should be around 0.62, but from the observation that (with the exception of Z CMa and MWC 342 as noted before) the emission should be bordered by absorption on the shortward side, another indication of a decelerating envelope according to our analysis. This leads us to use a uniform model for all the stars listed, i.e., a

TABLE 2

SPECTROMETRIC DATA

	Hβ				Hγ				Hδ			
STAR	Δv_r (km s^{-1})	$-\Delta v_b$ (km s^{-1})	$K(-\Delta v_r/\Delta v_b)$	Central Int.	Δv_r (km s^{-1})	$-\Delta v_b$ (km s^{-1})	K	Int.	Δv_r (km s^{-1})	$-\Delta v_b$ (km s^{-1})	K	Int.
BD+61°154.....	224	430	0.52	4.1	270	520	0.52	2.6	234	430	0.54	1.93
AB Aur.....	264	420	0.63	2.7	246	440	0.56	1.35	228	348	0.65	1.20
HD 31648.....	250	390	0.64	1.71	...	...	...	...	...	...	...	...
HD 250550.....	295	510	0.58	2.17	262	430	0.61	1.34	...	...	...	...
HD 50138.....	150	...	...	2.70	140	244	0.57	1.41	...	...	...	...
Z CMa.....	170	282	0.60	1.57	...	...	...	1.09	...	...	...	...
XX Oph.....	312	545	0.57	13.0	296	555	0.54	4.50	294	550	0.54	2.40
CoD−27°11944...	390	530	0.73	8.65	415	560	0.74	3.72	430	550	0.78	2.55
MWC 342.....	328	...	...	7.06	348	...	...	2.82	268	...	...	1.77

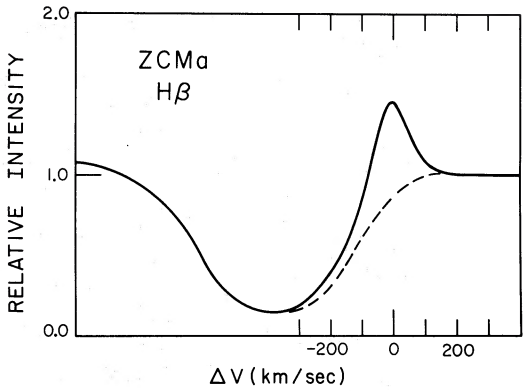

FIG. 9.—Observed Hβ profile of Z CMa. The dashed curve shows what the line profile would be in the absence of an expanding envelope.

velocity law $v \propto r^{-1/2}$ with the maximum velocity of expansion at the photosphere, which we take to be roughly the same as the observed velocity shift of the shortward edge of the spectral line. To save computation time, we have produced standard models at different stellar temperatures and equal luminosity of absolute magnitude -4 and having $v(r) = 300(R/r)^{1/2}$ km s^{-1}. Since most of the observed profiles are complicated by photospheric lines, we attempted only to compare the observed central intensities with the computed ones. For stellar temperatures less than 20,000 K, He was assumed to be singly ionized in the calculation of the electron densities. Again 12 levels of hydrogen were used. To find the mass loss for an observed star, the following procedure is used. The temperature and luminosity are obtained from sources independent of line profile calculations. It is assumed that the optical depth in the envelope is proportional to $\rho^2/(v/R)$, ignoring the variation of the departure coefficients with density (see e.g. [18a], $N_i^* \propto N_e N\rho \propto \rho^2$). Let Δm be the mass loss rate; then $\tau \propto (\Delta m)^2/(R^3 v^3)$. To produce the same profile for different R and v's, we must scale the mass loss rate Δm according to $\Delta m \propto (Rv)^{3/2}$. The model of a particular mass loss rate is chosen such that the computed intensities fit more closely the observed ones.

Table 3 shows the star's spectral type, approximate color temperature T_c (used in model calculations as the star's blackbody temperature and not to be confused with the observed effective temperature), and radius, calculated from the absolute luminosity and effective temperature whenever they are known or assumed appropriate to its spectral type of main-sequence luminosity. Strom *et al.* (1972) give the logarithms of the ratios of the luminosities of BD+61°154, AB Aur, and Z CMa to that of the Sun as 2.10, 1.83 and 2.96 respectively, which are all close to the main sequence, and the reference. Table 4 shows the comparison between observed and computed intensities.

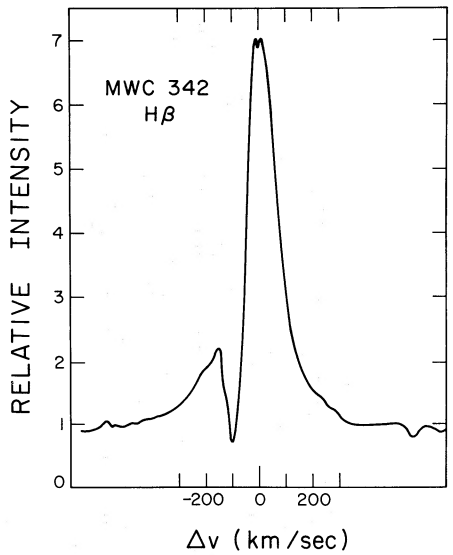

FIG. 10.—Observed Hβ profile of MWC342

TABLE 3

STELLAR DATA

Star	Sp. Type	T_e(K)	$R/R_\odot$	Reference
BD+61°154.....	B8	20,000	2.4	DM, S
AB Aur.....	B9	16,000	2.3	DM, S
HD 31648.....	A2	13,500	2.1	B
HD 250550.....	B7	20,000	3.2	
HD 50138.....	B8	20,000	3.0	B
Z CMa.....	B5	18,000	7.0	DM, S
XX Oph.....	A0	16,000	2.6	B
CoD−27°11944...	B8	20,000	3.0	B
MWC 342.....	B8	20,000	3.0	KK

NOTE.—DM = Dyck and Milkey 1972; S = Strom *et al.* 1972, B = Beals 1951, KK = Kleinmann and Kuhi 1972.

The agreement between observation and theory is not perfect, especially for the stars having strong emission lines. Part of the reason is certainly due to our crude theory, but it is also largely due to observational difficulties. The location of the continuum is quite uncertain. In the case of XX Oph, the error can be as large as 50 percent. When the emission is many times above the continuum, due to the extremely nonlinear photographic response the observed intensity is extremely uncertain. Therefore, large intensities of Hβ given in Table 4 should be viewed as being only qualitatively correct. Of course, we should also keep in mind that if these observed values are reliable, one should not hesitate to seek other theoretical explanations for the steep Balmer decrement of XX Oph. We should also like to remark that for all our models of stellar temperature ranging from 12,000 K to 30,000 K, none matches the observed rapid decrease in intensity. For the other comparisons between model and observation, we have good reason to believe that the agreements are within observational errors.

Another reason for choosing these stars for the determination of mass loss rates is that they are all of late B and early A spectral types, thereby having a narrow range in stellar temperature. If there were any correlation between infrared excess and mass loss rates, the effect caused by the temperature difference is then minimized. Unfortunately, there seems to be no obvious correlation simply between the mass loss rate and infrared excess, but instead there seems to be a fairly well-defined empirical relation between the infrared excess and the momentum flux, $(\rho v^2)_0$, at the base of the envelope.

Figure 11 is a plot of $(\rho v^2)_0$ versus the ratio of 10-μ to 2.2-μ fluxes which serves as a measure of infrared excess. The infrared measurements come from Kleinmann and Kuhi (1972) with the exception of those of HD 31648 and HD 50138 (Allen 1973), and HD 250550 (Cohen 1974). For HD 51480, we have used the profile plots of Beals (1951) to determine $(\rho v^2)_0$, and the infrared emission is taken to be optically thin free-free emission according to Allen (1973). The filled circle in the figure denotes dust reradiation (either circumstellar or associated with the nebulosity) and the × denotes free-free emission. All the types given are taken from Allen (1973) with the exception of those of XX Oph and CoD−27° 11944, which seem to have a free-free spectrum that becomes optically thick at 10 μ, according to the spectral distributions given by Kleinmann and Kuhi (1972).

Since the emission intensity is quite sensitive to the optical depth in the envelope, we do not expect much error in matching a model of certain optical depth to an observed profile. The error in determining $(\rho v^2)_0$ or f can be estimated as follows: $\tau \propto \rho_0^2 R/v_0 \propto (\rho v_0^2)^2 R/v_0^5 = f^2 R/V_0^5$; assuming the same τ for the same profile, we have $f \propto (v_0^5/R)^{1/2}$. The quantity v_0 can be measured to within 10 percent. If we know the luminosity within 3 magnitudes, the uncertainty in f can be at most a factor of 2. Since we have considered all stars to have approximately the same luminosity, a condition which is not unplausible, considering the fact that they have the common property

TABLE 4

COMPARISON BETWEEN OBSERVED AND COMPUTED INTENSITIES

Star	Mass Loss Rate ($10^{-6} M_\odot$ yr^{-1})	v_0 (km s^{-1})	Observed Intensity			Computed Intensity		
			Hβ	Hγ	Hδ	Hβ	Hγ	Hδ
BD+61°154.....	0.19	450	4.1	2.6	1.9	4.1	2.4	1.8
AB Aur.....	0.33	400	2.7	1.4	1.2	2.1	1.4	1.2
HD 31648.....	0.031	390	1.7	...	...	1.7	...	...
HD 250550.....	0.17	470	2.2	1.4	...	2.2	1.4	...
HD 50138.....	0.062	240	2.7	1.4	...	2.5	1.6	...
Z CMa.....	0.14	280	1.6	1.1	...	1.5	1.2	...
XX Oph.....	0.38	550	13.0	4.5	2.4	6.5	4.0	3.0
CoD−27°11944...	0.52	540	8.6	3.7	2.6	6.0	3.7	2.6
MWC 342.....	0.15	300	7.1	2.8	1.8	4.4	2.6	1.8

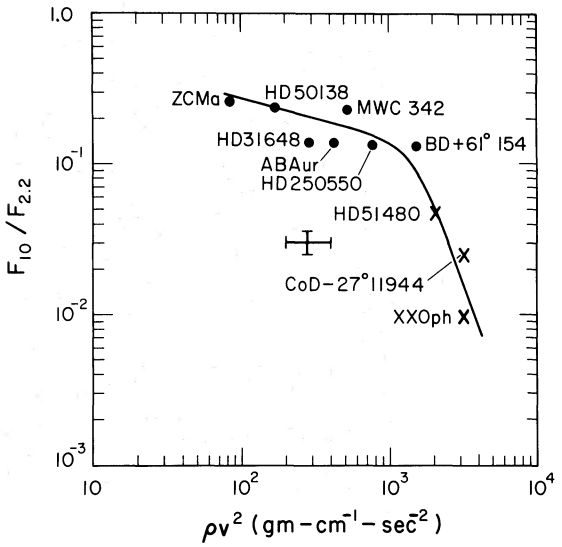

FIG. 11.—Ratio of 10-μ flux to 2.2-μ flux versus momentum flux, $(\rho v^2)_0$. *Filled circles*, dust; *crosses*, free-free emission.

of possessing P Cygni profiles, any uniform change in R for all stars will only shift the abscissa of Figure 11, which is on a logarithmic scale. In any case, assuming our model to be correct, an error of at most 0.3 in the log along the abscissa is not unreasonable. The observational errors in the ordinate, the infrared fluxes, are not greater than 20 percent. The range of points in Figure 11 covers more than 1 decade in the ordinate and almost 2 decades in the abscissa. Therefore the relation shown in Figure 11 can be considered to be well defined.

We also would like to note that for stars with low momentum fluxes, the infrared excesses are large and show a spectrum characteristic of dust reradiation, while for large momentum fluxes the infrared excesses decrease and the spectral distribution turns into free-free electron-ion emission.

IV. DISCUSSION

Much of the validity of the results presented earlier obviously depends heavily on the assumption of a decelerating envelope. This assumption is invoked in order to compute profiles of P Cygni type that have relatively narrow emission and deep absorption components. It can be considered purely phenomenological and ad hoc, but there are also strong reasons for believing that the assumption indeed gives a physical description of the outer atmospheres of P Cygni stars. Some of these reasons are outlined below.

It has been noted that the ratio of the velocity shifts of the longward and shortward edges from the central emission peak of a P Cygni profile is remarkably close to a constant for the stars we have studied. If our selection is typical of these stars, the above stated uniformity points to a symmetry in the line formation region, which can either be plane-parallel or spherical, otherwise the random orientation of stars to the line of sight will give rise to dissimilar profiles. If the former symmetry is a true description of the line formation region, then in order to have an emission line formed, the atmosphere must have a temperature inversion, or more precisely a source function inversion. In the absence of efficient pumping mechanisms for hydrogen, a source function inversion in fact implies a temperature inversion. Since most of the emission peaks have approximately the same velocity as the photospheric lines (usually weak lines from other nonhydrogen ions), the emission on their longward side comes from atoms moving away from the observer. In the plane-parallel case, it means either that the line formation region is contracting, which is impossible (since the shortward shifted absorption indicates expansion) or that the broadening is due to random thermal motion. Most of the P Cygni stars have emission widths of more than 100 km s^{-1} which would result in a temperature of several hundred thousand kelvins. The absence of spectral lines from highly ionized heavy metals rules out this possibility also. Therefore, we conclude that the emitting region must have spherical symmetry. Previously we have shown that in a spherically expanding atmosphere, intense emission and deep, wide absorption below the continuum (which is so characteristic of P Cygni profiles) are incompatible with the assumption of an accelerating atmosphere, and that the assumption of a decelerating atmosphere provides a natural explanation. We emphasize that spherical symmetry is important to the argument, for without it, arbitrary velocity structures can be invoked to also produce P Cygni–like profiles by assuming ejection of matter in appropriately positioned cones (Hutchings 1972).

A decelerating envelope model for P Cygni stars would come as a surprise to most workers in the field. Influenced by the successful prediction of the supersonic expansion of the solar wind by Parker (1958, 1960*a*, *b*, 1963) in his steady expansion theory, various workers have tried to establish theories for stellar winds. Among the

prominent works are those of Lucy and Solomon (1967, 1970), and Cassinelli and Castor (1973). All these theories require a steady expansion marked by monotonic acceleration through a critical point where the flow velocity equals the local sound velocity. For the Sun, the existence of a hot and tenuous corona makes such a solution possible. For early type stars which show emission lines, and where the outer atmosphere can be estimated to have quite high densities ($\sim 10^{11}$ particles cm^{-3}), there has been no conclusive proof that a hot corona exists. The only way to achieve a Parker-type solution is to increase the radiative pressure gradient or to add heat to the expanding envelope so that in the supersonic region the effective gravity becomes negative. (This statement can be verified easily by considering the equations given below.) Lucy and Solomon considered removal of ultraviolet photon momentum by resonant line scattering, and Cassinelli and Castor pointed to the importance of absorptive opacity in driving more mass out. In a region where the radiation field is decoupled from the gas, the differential equation governing the gas flow with spherical symmetry can be written as

$$\frac{dv}{dr} = \frac{v}{r}\left(\frac{2v_s^2 - rg_{\rm eff} - rv^{-1}Q}{v^2 - v_s^2}\right), \tag{23}$$

where v and r have their usual meanings, v_s is the local sound velocity, $g_{\rm eff}$ the effective gravity, and Q a term related to the heat input per unit mass. The corresponding plane-parallel equation can be obtained by letting $r \to \infty$ on the right-hand side of (23) (the term $2v_s^2$ will then disappear). The quantity $g_{\rm eff}$ is given by

$$g_{\rm eff} = \frac{GM}{r^2} - \frac{\kappa L}{4\pi r^2 c}, \tag{24}$$

where M is the stellar mass, G the gravitational constant, L the luminosity, and κ the averaged mass absorption and scattering coefficient averaged over the spectrum of the star.

A steady flow solution to the problem of supersonic expansion applied to P Cygni type stars can raise several objections. First, for small subsonic velocities in the absence of heat input, since $dv/dr \propto v$, it leaves the energization of the flow unexplained. Second, the opacity must vary through a large range in order to accelerate the material to hypersonic velocities. The luminosity must be high enough that the outward radiation force eventually overtakes that of gravity. P Cygni itself is quite luminous, and such a solution may be plausible; but for the other stars we have studied, whenever there are reliable data, they are shown to lie closer to the main sequence. If they have masses comparable to main-sequence stars, it is very unlikely that the effective gravity can ever be negative.

We can take another look at equation (23) and relax the condition that the material is accelerated smoothly through the critical point when the numerator and denominator vanish simultaneously. For hypersonic velocities, $v \gg v_s$, and v_s can be neglected in the equation. This is equivalent to neglecting the gas pressure. Let us also assume that the gas has moved away from the ejecting region and heat input has become insignificant. Then the velocity structure becomes

$$v = (c_1 + 2(GM - \kappa L/4\pi c)(r)^{1/2}, \qquad v \gg v_s. \tag{25}$$

If the effective gravity is positive and constant through the region, and if the constant of integration, c_1, is zero, this is precisely the velocity law we derived from line profile fitting. The physical picture is that the envelope is ejected from the star by some as yet unknown mechanism and subsequently slows down under gravity. It is this outer decelerating layer of the envelope that gives the observed P Cygni profiles.

The agreement between the velocity laws derived from line profile fitting and from a particular solution of the flow equation may be fortuitous, but at least its simplicity deserves attention. It also makes sense in the interpretation of the result shown in Figure 11 where the infrared excess is plotted against the maximum momentum flux, $(\rho v^2)_0$. Let us suppose that a fraction f of the momentum flux is left after the envelope expands to large distances. Then the plot in Figure 11 will still have the same shape if we replace $(\rho v^2)_0$ by $f(\rho v^2)_0$ which may be quite a small number. Suppose dust is present around the star before the ejection of the envelope. Large momentum flux $f(\rho v^2)_0$ will tend to drive away the dust or create shock waves disintegrating the dust, but small $f(\rho v^2)_0$ may leave the dust undisturbed. It is also quite possible that dust is formed from the ejected matter and remains around the star if the momentum flux is not enough to disperse it. From Figure 11 we see that small $(\rho v^2)_0$ corresponds to large infrared excess and the presence of dust while large $(\rho v^2)_0$ corresponds to free-free emission. We have also examined spectra in which the hydrogen lines are in pure emission, an indication of no appreciable deceleration, and checked the star's infrared spectrum from the list given by Allen (1973). All such stars belong to the free-free class. This also fits our picture that large momentum fluxes tend to prevent the presence of dust around those stars. Since we do not have a large number of points on the graph, the results should be considered preliminary.

It is well known that P Cygni was discovered as a nova in 1600 and underwent irregular changes in brightness until it settled down to its present state more than a hundred years later. Nearly all the P Cygni stars listed by Beals (1951) show spectral changes, especially in the strength of the emission lines. Random short-term variation in spectral features have also been observed by Hutchings (1971) and Rosendhal (1973). In view of the variability, it is not clear how much emphasis one should place on a theory of steady expansion through a critical point. It would seem that a violent ejection mechanism might be more suitable for these stars, but theories of this kind are still

lacking. Shock-induced acceleration has been investigated for the Sun (Stein and Schwartz 1972), but it remains to be seen whether it can be applied to P Cygni stars.

Recently Wendker, Baars, and Altenhoff (1973), from radio interferometric measurements, determined the angular size of the radio emitting region of P Cygni to be less than 2″. From a standard distance assigned to P Cygni (1200 pc) and the time of outburst about 300 years ago, they deduced an expansion velocity of the outer boundary to be less than 40 km s^{-1}. Whether this supports our theory of deceleration under gravity or subsequent slowdown through shock dissipation cannot be uniquely ascertained at present.

Despite our fitting of the strong Balmer lines of P Cygni and predicting the observed Balmer decrement, our model suffers from crudity and several omissions. We have identified the star as a sphere emitting blackbody radiation. In moving atmospheres, it is not at all clear that a normal photosphere has any meaning. We have simply assumed a sharp boundary between the star and the expanding envelope. Only lines formed in the moving envelope are computed. In the case of decelerating atmospheres, the mechanism of acceleration of the envelope to the escape velocity is ignored. Weak lines, especially lines from different ions at different excitations, are likely to be formed deep in the atmosphere where the acceleration takes place, and so our model of decelerating envelopes must break down completely. It is only through the study of the formation of these lines that a complete picture of the atmospheres of P Cygni stars can be obtained.

If our picture of a decelerating envelope is correct, we can estimate the mass of the star by measuring the maximum expansion velocity, since it must be greater than or equal to the escape velocity of the star. Of course, we do not know where the maximum velocity occurs in relation to the center of the star. For the stars we have studied (except P Cygni) if we assume this distance to be 5 $R_\odot$, the masses range from about 1 to 5 $M_\odot$. For P Cygni if we take R to be 15 $R_\odot$, the mass turns out to be around 8 $M_\odot$ If these values are reliable, then they are rather less massive than normal stars of the same spectral types. This indicates that they might have shed a sizable fraction of their mass in the course of their evolution.

V. SUMMARY

The presence of P Cygni profiles in the spectra of stars is interpreted as being due to the existence of extended expanding atmospheres around these stars. The velocity of expansion is usually several hundred km s^{-1}. This is much higher than the random thermal velocity, so that the Sobolev approximation of line formation in a moving atmosphere is appropriate. In this approximation, different points on a profile are formed on their corresponding velocity surfaces in the expanding envelope. Because of the geometry of the velocity surfaces, an accelerating atmosphere gives a profile that has little or no absorption below the continuum if the emission is very strong; a decelerating atmosphere gives a profile that has a relatively narrow emission component, a consequence of the occultation by the stellar core; and a deep absorption component if the opacity in the envelope is high. Spherically expanding atmospheres are assumed in deriving the above results.

Non–LTE determination of hydrogen level populations has been carried out (using Castor's escape probability method). If there are no drastic changes in temperature in an envelope of moderate density ($\sim 10^{11}$ particles cm^{-3}), the level populations of H are largely determined by photoionization from the ground state followed by subsequent recombination to the higher levels. By assuming a constant mass ejection rate, spherical symmetry, and a particular velocity structure, the number densities of each level of hydrogen (we have taken 12 levels) is determined throughout the envelope. From analysis of the profile characteristics of P Cygni, we have taken a velocity structure $v \propto r^{-1/2}$. Numerical computation of the hydrogen profiles gives a quite satisfactory fit to the observed profiles. The mass loss rate of P Cygni is found to be about $3.4 \times 10^{-6}\ M_\odot\ yr^{-1}$, assuming a composition of 64 percent H and 36 percent He by mass.

The mass loss rates of a number of other P Cygni stars are determined by fitting the Balmer emission intensities. When the momentum flux is correlated with the observed infrared excesses, it is found that low momentum flux gives high infrared excess with a spectrum characteristic of dust emission, whereas high momentum flux gives low infrared excess with a free-free electron-ion emission spectrum. This indicates either that dust is unable to form in a stream of gas of high momentum or that it is being blown away by the mass flux.

The model of decelerating outer envelopes for P Cygni stars raises the question of the ejection mechanism. Traditionally a Parker-type solution is favored. It gives steady monotonic acceleration through the sonic point up to very high Mach numbers and does not allow subsequent slowdown unless there is a shock transition. Our result suggests a violent ejection mechanism and subsequent slowdown under gravity which may still be the dominant force in the outer envelope. Since we do not have a theory of mass ejection, the velocity structure derived from profile fitting should be considered preliminary even though radio infrared observations also point to the plausibility of such a structure.

We would like to thank Drs. J. Silk and J. Scargle for critical comments and helpful discussions, and Dr. M. Cohen for instructive information on infrared observations. This research was supported in part by National Science Foundation grant GP-30342.

REFERENCES

Allen, C. W. 1963, *Astrophysical Quantities* (London: Athlone Press).
Allen, D. A. 1973, *M.N.R.A.S.*, **161**, 145.
Beals, C. S. 1929, *M.N.R.A.S.*, **90**, 202.
———. 1930, *Pub. Dom. Ap. Obs.*, **4**, 271.
———. 1931, *M.N.R.A.S.*, **91**, 966.
———. 1934, *Pub. Dom. Ap. Obs.*, **6**, 111.
———. 1951, *ibid.*, **9**, 1.
Caroff, L. J., Noerdlinger, P. D., and Scargle, J. D. 1972, *Ap. J.*, **176**, 439.
Cassinelli, J. P., and Castor, J. I. 1973, *Ap. J.*, **179**, 189.
Castor, J. I. 1970, *M.N.R.A.S.*, **149**, 111.
Castor, J. I., Smith, L. F., and van Blerkom, D. 1970, *Ap. J.*, **159**, 1119.
Chandrasekhar, S. 1934, *M.N.R.A.S.*, **94**, 522.
Cohen, M. 1974, private communication.
Dyck, H. M. and Milkey, R. W. 1972, *Pub. A.S.P.*, **84**, 597.
Geisel, S. L. 1970, *Ap. J.* (*Letters*), **161**, L105.
Gerasmovic, B. 1933, *Zs. f. Ap.*, **7**, 335.
———. 1935, *ibid.*, **10**, 154.
Hutchings, J. B. 1968*a*, *M.N.R.A.S.*, **141**, 219.
———. 1968*b*, *ibid.*, p. 329.
———. 1969, *ibid.*, **144**, 235.
———. 1971, in Colloquium on Supergiant Stars, Trieste.
———. 1972, *M.N.R.A.S.*, **158**, 177.
Johnson, H. L. 1967, *Ap. J.* (*Letters*), **150**, L39.
Kleinmann, S., and Kuhi, L. V. 1972, *Pub. A.S.P.*, **84**, 766.
Kopylov, I. M. 1958, *Izv. Krymsk. Ap. Obs.*, **20**, 156.
Kuhi, L. V. 1964, *Ap. J.*, **140**, 1409.
———. 1973, *ibid.*, **180**, 783.
Lucy, L. B. 1971, *Ap. J.*, **163**, 95.
Lucy, L. B., and Solomon, P. M. 1967, *A.J.*, **72**, 310.
———. 1970, *Ap. J.*, **159**, 879.
Lyong, L. V. 1967, *Soviet Astr.—AJ*, **11**, 224.
Magnan, C. 1970, *J. Quant. Spectrosc. and Rad. Transf.*, **10**, 1.
———. 1972, *Astr. and Ap.*, **21**, 361.
Mihalas, D. 1970, *Stellar Atmospheres* (San Francisco: Freeman).
Morton, D. C. 1967*a*, *Ap. J.*, **147**, 1017.
———. 1967*b*, *ibid.*, **150**, 535.
Morton, D. C., Jenkins, E. B., and Bohlin, R. C. 1968, *Ap. J.*, **154**, 611.
Morton, D. C., Jenkins, E. B., and Brooks, N. H. 1969, *Ap. J.*, **155**, 875.
Noerdlinger, P. D., and Scargle, J. D. 1972, *Ap. J.*, **176**, 463.
Parker, E. N. 1958, *Ap. J.*, **128**, 664.
———. 1960*a*, *ibid.*, **132**, 175.
———. 1960*b*, *ibid.*, p. 821.
———. 1963, *Interplanetary Dynamical Processes* (New York: Interscience).
Percival, I. C. 1966, *Nucl. Fusion*, **6**, 182.
Rosendhal, J. D. 1973, *Ap. J.*, **182**, 523.
Rottenberg, J. A. 1952, *M.N.R.A.S.*, **112**, 125.
Rublev, S. V. 1961, *Soviet Astr.—AJ*, **4**, 780.
———. 1964, *ibid.*, **7**, 492.
Rybicki, G. B. 1970, in *Spectrum Formation in Stars with Steady-State Extended Atmospheres*, (*NBS Special Pub.*), 332.
Sobolev, V. V. 1958, in *Theoretical Astrophysics*, ed. V. A. Ambartsumian (New York: Pergamon Press).
———. 1960, *Moving Envelopes of Stars* (Cambridge: Harvard University Press).
Stein, R. F., and Schwartz, R. A. 1972, *Ap. J.*, **177**, 807.
Strom, S. E., Strom, K. M., Yost, J., Carrasco, L., and Grasdalen, G. 1972, *Ap. J.*, **173**, 353.
Wendker, H. J., Baars, J. W. M., and Altenhoff, W. J. 1973, *Nature Phys. Sci.*, **245**, 118.
Wilson, O. C. 1934, *Ap. J.*, **80**, 259.

P. KUAN: Kitt Peak National Observatory, 950 N. Cherry Avenue, Tucson, AZ 85726

L. V. KUHI: Astronomy Department, University of California, Berkeley, CA 94720